



ELSEVIER

Physica A 267 (1999) 98–110

PHYSICA A

Anisotropic plasticity with embedded-atom potentials

Wm.G. Hoover^{a,*}, Siegfried Hess^b^a*Department of Applied Science, University of California at Davis/Livermore, and Lawrence Livermore National Laboratory, Livermore, CA 94551-7808, USA*^b*Institut für Theoretische Physik, Technische Universität Berlin, Hardenbergstrasse 36, Berlin 10623, Germany*

Received 2 December 1998

Abstract

Embedded-atom potentials are a useful supplement to pair potentials in the modelling of defects and metal plasticity. Here we emphasize the steady isothermal shear deformation of two-dimensional models made up of many interacting grains. The embedded-atom-plus-pairs potential can provide very anisotropic grains, which are oriented by the shear deformation. We simulate plastic shear deformation, at fixed density and temperature, with the Sllod and Doll's-Tensor algorithms. We explore the temperature-dependent elastic and plastic moduli for two relatively anisotropic models with static anisotropies similar to those of the coinage and alkali metals. In both cases the flow stress is relatively insensitive to strain rate at moderate strain rates. At high strain rates shear bands develop. © 1999 Elsevier Science B.V. All rights reserved.

PACS: 05.60+w; 46.10.+z; 66

Keywords: Plasticity; Anisotropy; Nonequilibrium molecular dynamics

1. Introduction

Computer simulations of solid-phase plastic flow and fracture have been carried out with as many as 10^8 atoms in state-of-the-art molecular dynamics simulations [1]. Such work presents two difficulties. First, the visualization and analysis of such a large simulation is a major undertaking [2], hence extracting the physics is difficult [3]. Second, it is hard to draw general conclusions from the computed results because the potentials

* Corresponding author. Fax: 1-925-422-8681.

E-mail address: hoover@bonampak.llnl.gov (Wm.G. Hoover)

chosen are typically fitted to the properties of particular materials. Here we are interested in developing models which can exhibit a wide range of constitutive properties. As a part of this work we are developing algorithms for the simulation and study of anisotropic granular materials. The studies we report here are in two dimensions. Our intention was to produce relatively simple results. In fact, the flow morphologies we found are fairly complicated, and show a transition from a relatively homogeneous deformation to a heterogeneous shear band formation at strain rates comparable to those found in strong shock waves. Despite this unexpected complexity, there are no additional special difficulties, other than visualization, as mentioned above, in extending the present two-dimensional ideas and models to three-dimensional applications.

There is a need for understanding the behavior of anisotropic granular materials under complex loads. This need can best be met by the study of simple models. It is desirable to have an atomic scale mechanical model underlying the analysis, providing a conceptual basis for flow properties, so as to avoid *ad hoc* constitutive assumptions. Even in the simplest cubic-symmetry metals, such as gold and potassium, there is strong anisotropy, with the two shear moduli C_{44} and $(C_{11} - C_{12})/2$ differing by factors of three and seven, respectively. We consider two detailed models, with anisotropies similar to these, in what follows. To build an understanding of the flow properties of such metals, we must invent atomistic potential functions able to provide strongly anisotropic mechanical properties. The embedded-atom approach [4–6], which is closely related to smooth-particle methods [7–9] for continuum simulations, provides a useful starting point. Effects of impurities as well as the inhomogeneities induced by the freezing process can readily be introduced.

A quantitative study of real granular crystals would require a special treatment for the grain surfaces, where impurities concentrate, and enhance or retard deformation. Here we consider more idealized systems, in which “grains” of material are generated dynamically, by the deformation itself, and have the same composition as the bulk. This idealized situation should describe physical situations in which the deformation process is faster than competing diffusive processes.

The two-dimensional triangular lattice, with six nearest neighbors and six-fold rotational symmetry, is necessarily elastically isotropic, with C_{44} and $(C_{11} - C_{12})/2$ equal, so that a first goal is to stabilize the potentially *anisotropic* square-lattice structure relative to the triangular lattice. In three dimensions, this goal is analogous to stabilizing the body-centered cubic structure, or even the simple-cubic and diamond structures, relative to the close-packed structures. In the paper we describe a general family of models, all with short-ranged forces based on pair sums, but with explicit many-body embedded-atom effects included. These models can stabilize either of the two-dimensional simple lattices and make it possible to vary the elastic anisotropy as well.

Because knowing elastic constants requires only the time averaging of certain lattice sums, the elastic properties of simple crystal structures are familiar long-standing results of computer simulation [10,11]. Simulating plasticity requires an additional thermostatting mechanism to extract the irreversible heating. The plastic deformation

of two-dimensional solids at high strain rates used Gauss' Principle to fix the temperature of far-from-equilibrium shear flows [12]. That 1982 work, which treated short-ranged pair potentials, in the isotropic triangular-lattice structure, gave rise to relatively-simple, but temperature-dependent, power-law relations linking the stationary plastic shear stress to the strain rate. Over the feasible range of strain rates, about two orders of magnitude, the stationary flow stress varied as a power of the strain rate: $\sigma \propto \dot{\epsilon}^{p(T)}$, with the temperature-dependent power $p(T)$ increasing from $\frac{1}{8}$ to $\frac{1}{3}$ as the temperature was increased. The latter power is also consistent with some more recent shockwave studies [13] as well as studies carried out at more moderate rates [14].

There is no present theoretical understanding for the observed constitutive behavior, at high strain rates, of systems governed by pairwise-additive forces. It is therefore, not at all obvious how to predict the equation of state and yield behavior of anisotropic *granular* crystals, even though very similar nonequilibrium simulation techniques can be applied to them. Such a problem, where theoretical understanding is quite limited, but simulation is possible, is ideally suited to nonequilibrium molecular dynamics. With these problems in anisotropic plasticity in mind we have carried out quenching simulations on systems of particles designed to prefer the square lattice arrangement, and studied the response of these models to both elastic and plastic deformations. We have considered the details of two models, with anisotropies (ratio of the maximum to the minimum shear modulus) of four and eight.

2. Anisotropy from embedded-atom potentials

Daw and Baskes [4] originated the embedded-atom treatment of metals. Because pair potentials imply (i) the equality of the stress-free static elastic constants C_{12} and C_{44} , as well as (ii) the approximate equality of the binding energy and the vacancy energy, while real metals are typically far from satisfying either equality, it is natural to extend the pair force concept to include collective embedding contributions. In addition to the usual pair potentials familiar from kinetic theory and rare gas simulations, their total potential energy Φ includes collective "embedding" functions $\{F(\rho)\}$ of the individual particle densities, which are computed as local electronic-density sums:

$$\Phi = \sum_{i < j} \phi_{ij} + \sum_i F(\rho_i); \rho_i = \sum_j w(r_{ij}).$$

The embedding function represents the electronic binding energy of a metal core to its local environment. The electronic densities are calculated by superposition, using individual atomistic functions which closely resemble the "weight functions" used in "smooth particle applied mechanics". This latter technique, "SPAM" for short, was discovered by Monaghan and Lucy in 1977 [7,8], and uses *particles* to represent continuum properties, with their time development providing a convergent solution to the macroscopic continuum equations. Smooth-particle simulations proceed by computing and advancing the continuum field variables, like energy and stress, based on

contributions from neighboring particles lying within the range h of the weight function $w(r < h)$.

Simulations of macroscopic continuum flows, using smooth particle applied mechanics, have shown very interesting arrangements of particles, much more varied than those associated with simple pair potentials [15]. This structural variability is attractive for the modeling of metals, though a bit overwhelming in its generality. Accordingly we here consider two-dimensional systems, choosing a combination of a pair potential ϕ , a weighting function $w(r)$, and a density functional F which stabilizes the square lattice structure at low temperature.

We began with a simple short-ranged pair potential $\chi(r < h)$,

$$\chi(r < h) = 3(h - r)^4 - 4(h - 1.0)(h - r)^3 ,$$

with a minimum energy of $-(h-1)^4$ at a separation of 1. We have chosen the maximum range of the potential, $h=1.8$, so as to include the second-neighbor interactions required to stabilize the square lattice. Along with the energy and length scales from the potential we fix the mass and temperature scales by choosing the atomic mass and Boltzmann's constant equal to unity too. The smooth cutoff of χ , at $r=h$, with two derivatives vanishing, was chosen to facilitate numerical simulations. Exploratory studies suggested further widening of the attractive bowl of the pair interaction, so as to favor the open square-lattice structure. Accordingly, we came to consider the family of pair potentials:

$$\phi(r < h) \equiv \chi(r)[1 + \alpha[\chi(r) - \chi(1)]] .$$

When this family of pair potentials is used in conjunction with a simple density functional $F = \sum(\rho_i - 1.0)^2$, where the individual particle densities $\{\rho\}$ are computed using Lucy's weight function over the range of values $\{0 < r < h\}$:

$$w(r < h) = (5/\pi h^2)[1 + 3(r/h)][1 - (r/h)]^3 ,$$

the two square-lattice shear moduli vary as is shown in Fig. 1. Outside the range shown in the figure, the triangular lattice becomes energetically relatively stable. We have chosen the two values $\alpha = (\frac{2}{3}, 1)$, for which the square lattice is stable, both mechanically and thermodynamically, with corresponding anisotropies $(C_{11} - C_{12})/(2C_{44}) \simeq (4, 8)$. For these α values, the energy difference between the square and triangular lattices is of the order of the thermal energy at melting, and, as is described in more detail below, the triangular lattice is itself unstable, mechanically, as well as thermodynamically.

Equilibrium and nonequilibrium (driven and thermostatted) simulations with the two embedded-atom potentials $\alpha = (\frac{2}{3}, 1)$, were carried out in the usual way [16,17]. We used a linked list of interacting pairs of particles to save time and a fourth-order Runge-Kutta integrator to preserve accuracy. Following exploratory free-boundary studies of crystal structure and location of the stress-free density, the more-usual periodic boundaries and nonequilibrium thermostat techniques were used to study bulk specimens. Fig. 2 shows typical quenched free-boundary specimens, achieved by cooling initial square lattices of 4096 particles to a temperature of 0.007. The grains show a width on the order of 20 particle diameters. Fig. 3 shows a typical granular structure, predominantly square

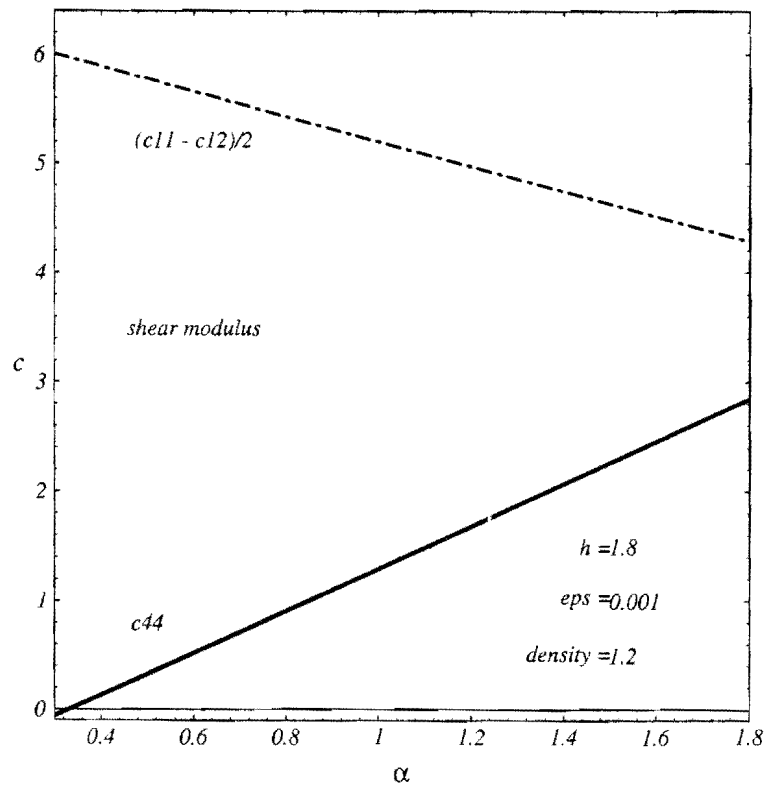


Fig. 1. Variation of the static zero-pressure shear moduli with the parameter α . Throughout the range plotted the square lattice structure is favored, energetically, over the triangular lattice structure. The anisotropy is characterized by the ratio of the larger to the smaller modulus. Our simulations used the values $\alpha = (\frac{2}{3}, 1)$ corresponding to anisotropies of eight and four.

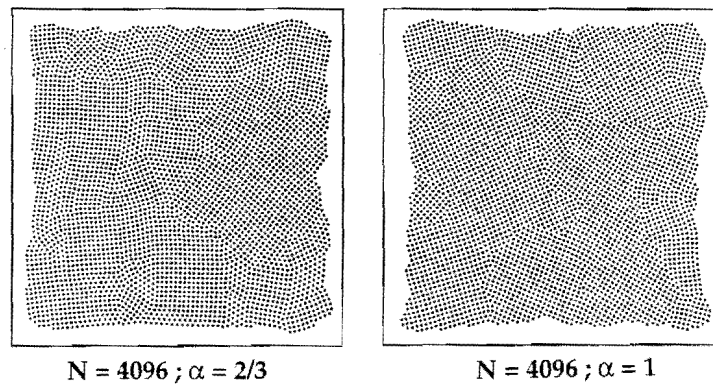
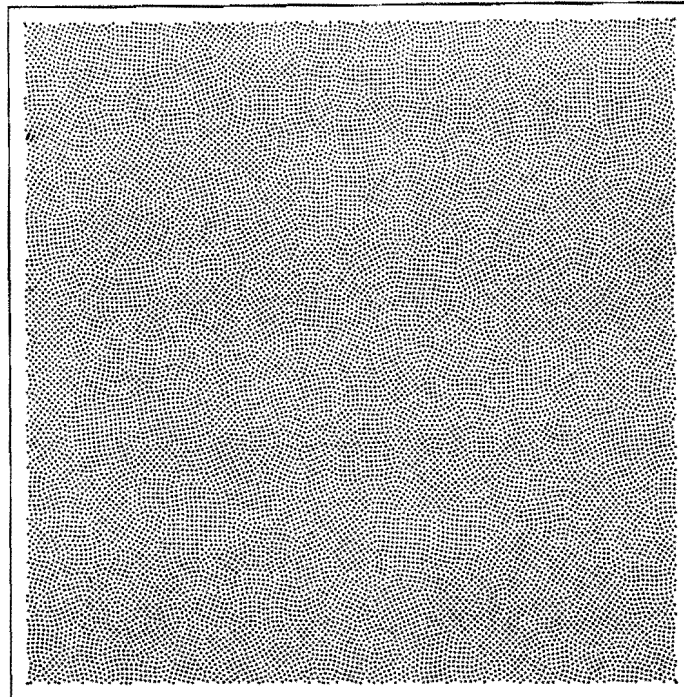


Fig. 2. Free-standing granular crystallites of 4096 particles, interacting with the embedded-atom potentials described in the text ($\alpha = \frac{2}{3}$ at left and $\alpha = 1$ at right) and quenched with a frictional force, $\dot{v} = -0.1v$ for a time of 100. The potential energies are $(-1.442, -1.474)$ per particle in the two cases. The static bulk perfect-crystal energies are $(-1.474, -1.511)$.



$N = 19\,660 ; \alpha = 2/3$

Fig. 3. Typical configuration of 19 660 particles, using the potential function of Fig. 2 with $\alpha = \frac{2}{3}$, after quenching. The potential energy per particle is -1.457 . The static bulk perfect-crystal energy is -1.474 .

lattice, generated by gradually cooling the fluid from a temperature of approximately twice the melting temperature. Although slower cooling results in a larger grain size, our interest in stationary shear processes, which determine a characteristic grain size as a function of strain rate, made a detailed study of the dependence of grain size on rate of quenching unnecessary.

In view of the difficulty in determining accurate solidification temperatures for two-dimensional systems with soft forces, we made no special effort to determine the precise equilibrium phase diagram for the models. Instead, we estimated the melting points by following the annealing of samples with about 2000 particles, started out with an artificial elastic strain [$\varepsilon_{yy} = -\varepsilon_{xx} = 0.1$], and then followed for a reduced time of 100, which corresponds to about seven sound-traversal times. Both models $\alpha = (\frac{2}{3}, 1)$ exhibit a clear solid structure at a temperature of 0.03 and a different disorderly fluid structure, with much smaller shear stresses, at a temperature of 0.06. The stiffer of the two materials $\alpha = 1$ is evidently solid at temperatures of 0.05 and 0.04, while the softer material has melted at these same temperatures. In Fig. 4 we compare the final configurations obtained in these relaxation studies for the two temperatures (0.03, 0.06). At the lower temperature, the residual shear stress and the degree of order are both larger for the stiffer crystal ($\alpha = 1$), suggesting that this material will display a larger dynamic yield strength. Our numerical yield strengths differ by roughly a factor of two, which is the ratio of the softer shear moduli of the two materials. With our solid-phase

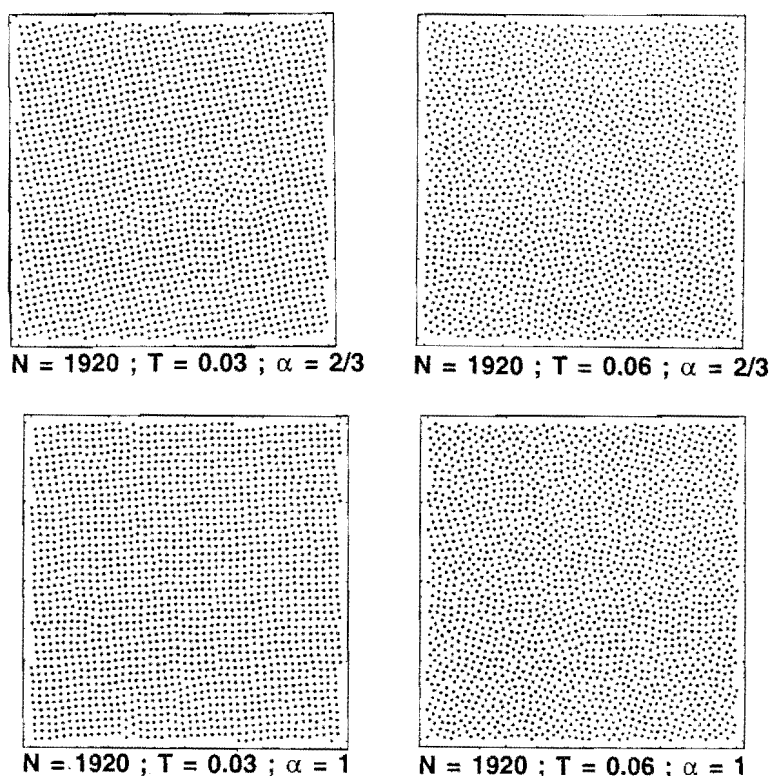


Fig. 4. Systems annealed for a total time of 100, about eight sound traversal times, with $\alpha = (\frac{2}{3}, 1)$ and temperatures of (0.03, 0.06). Stress histories suggest that the lower temperature corresponds to a stable solid phase.

stability evidence in mind we carried out solid-phase shear studies for the temperatures (0.01, 0.02, 0.03), anticipating that this range would roughly correspond to that studied earlier, using simple pair potentials, in Ref. [12].

3. Solid structure and moduli

The weight functions used in SPAM simulations can generate a host of complex structures, but the special cases we chose here, when used in conjunction with our relatively-soft pair potential, both favor the square lattice at low pressure. We determined the static thermodynamic properties of the square and triangular lattices by working out standard sums, checking the formal expressions involving forces with finite-difference calculations using extrapolated values from small strains, of order 0.0001–0.01. The bulk binding energies per particle and the bulk and shear moduli for the two models are listed in Table 1. For comparison, the (higher) binding energy of the (unstable) triangular lattice is shown at the same density.

The moduli for our two-dimensional crystals are analogs of their three-dimensional relatives. C_{44} describes the response of the shear stress σ_{xy} to the infinitesimal shear

Table 1

Energies per particle, E/N , bulk and shear moduli, for the square lattice, using the two embedded-atom potentials described in the text. The energy of the (unstable) triangular lattice at this same static-lattice density is given for comparison

α	ρ	$(E/N)_{\text{sq}}$	B	C_{44}	$(C_{11} - C_{12})/2$	$(E/N)_{\text{tri}}$
$\frac{2}{3}$	1.202	-1.474	9.85	0.66	5.60	-1.444
1	1.213	-1.511	10.40	1.37	5.36	-1.443

deformation:

$$(x, y) \rightarrow (x + \varepsilon y, y), \quad C_{44} \equiv \sigma_{xy}/\varepsilon.$$

The same deformation, applied to a crystal rotated through an angle $\frac{\pi}{4}$ generates a shear stress proportional to the modulus $(C_{11} - C_{12})/2$. A simple numerical computation distorts the original lattice without rotation:

$$(x, y) \rightarrow (x + \varepsilon x, y - \varepsilon y), \quad (C_{11} - C_{12})/2 \equiv (\sigma_{xx} - \sigma_{yy})/4\varepsilon.$$

4. Solid-phase plasticity

Beginning with a variety of different structures, we have generated dynamic granular structures by imposing a steady isothermal shear on these structures, using a friction coefficient ζ to fix the sum of the velocity fluctuations relative to the mean flow (“homogeneous thermostatting”). There are many ways to accomplish this. The two most common algorithms, Doll’s and Sllod [12,16,17], can both be expressed by the following set of $4N$ ordinary differential equations:

$$\{\dot{x} = p_x/m + \dot{\varepsilon}y; \dot{p}_x = F_x - C_1\dot{\varepsilon}p_y - \zeta p_x; \},$$

$$\{\dot{y} = p_y/m; \dot{p}_y = F_y - C_2\dot{\varepsilon}p_x - \zeta p_y; \},$$

where the constants (C_1, C_2) are $(0, 1)$ for Doll’s algorithm, and $(1, 0)$ for Sllod. Doll’s tensor gets its name from the qp “Kewpie” contribution in the underlying Hamiltonian,

$$\mathcal{H}_{\text{Doll}} = \mathcal{H}_0 + \sum \dot{\varepsilon} : qp.$$

“Sllod” is an Australianism invented by Denis Evans.

Exploratory simulations, like those in Ref. [12], with about 500 particles, proved to be too small, scarcely large enough to contain more than a single grain. Despite this these small-system simulations had mean shear stresses only a little larger than those of larger systems containing many grains. Although systems four times larger, with about 2000 particles, are adequate in most cases, we have chosen to present here data characterizing somewhat larger systems of about 8000 particles, using run lengths which correspond to about seven sound traversal times, which are adequate, in most cases. We give a selection of results in Tables 2 and 3, listing time-averaged values

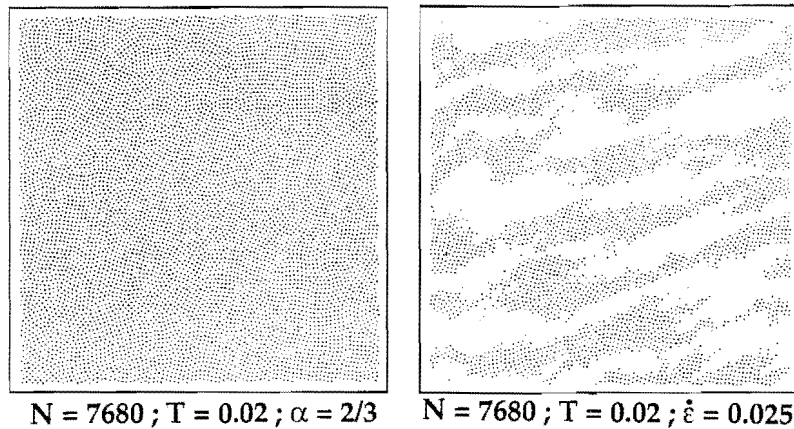


Fig. 5. Typical configuration of 7680 particles with $\alpha = \frac{2}{3}$ under Doll's-tensor shear at a temperature of 0.02 and a strain rate of 0.025. The potential energy per particle is -1.437 and the shear stress is 0.029. We include a view of those particles originally occupying the right-hand side of the periodic square in order to visualize the relative motions associated with the shearing.

of the stress-tensor components and the energy per particle as functions of strain rate $\dot{\epsilon} = \langle du_x/dy \rangle$ and temperature.

Fig. 5 includes two views of a typical low-temperature shear deformation, using 7680 particles at a strain rate 0.025 and temperature 0.02. In addition to the overall view we have plotted separately those particles which initially occupied the right-hand side of the periodic square container. This emphasizes the extreme plastic deformation which the simulated solids undergo (Table 2).

These simulations soon established that, except at very high strain rates, where the algorithms require relatively large rates of heat extraction through the friction coefficient ζ , there is little significant difference between the two simulation types, Doll's and Sllod. We compare both types in only a few cases. The practical range for computer simulations of such plastic flows is limited to two or three orders of magnitude, with the rates corresponding to the deformation rates expected in moderate to strong shock waves. At the highest strain rates, of order unity, there is a universal tendency toward shearband formation, with a loss of the homogeneous structure which characterizes the lower rates. Shear banding leads to a substantial reduction in the effective yield strength-by as much as a factor of two in for the stiffer of our two models, ($\alpha = 1$) (Table 3). Both simulation types and both potentials indicate dynamic yield strengths on the order of a few percent of the smaller of the two shear moduli, C_{44} .

The results found here for the stiffer potential ($\alpha = 1$) are much less sensitive to strain rate than those for ($\alpha = \frac{2}{3}$), with both σ_{xy} and $\tau = [\sigma_{xy}^2 + (\frac{1}{4})(\sigma_{xx} - \sigma_{yy})^2]^{1/2}$ much more sensitive to temperature than to strain rate. Until shear bands are formed, the softer potential shows a rate dependence resembling that of corresponding simulations with pairwise-additive forces [10]. In all of our simulations, the direction of the principal stress axis (the direction of maximum tension in the flowing solid) lags behind the flow. In recent Couette-flow simulations of fluid shear, using a soft repulsive potential, the direction of maximum shear stress likewise lagged the flow. The constitutive complexity

Table 2

Dependence of the stress tensor and energy on strain rate and temperature for simulations with 7680 particles ($\alpha = \frac{2}{3}$ and density 1.2). K represents the kinetic temperature per particle. The subscripts D and S indicate the simulation type, Doll's or Sllod. The individual run lengths are to a time of 240, with the first 40 time units discarded

N	$\dot{\epsilon}$	σ_{xy}	σ_{xx}	σ_{yy}	K	Φ
7680 _D	0.005	0.029	-0.078	-0.057	0.01	-1.457
7680 _D	0.005	0.023	-0.103	-0.083	0.02	-1.446
7680 _D	0.005	0.020	-0.130	-0.111	0.03	-1.436
7680 _D	0.010	0.035	-0.098	-0.069	0.01	-1.453
7680 _S	0.010	0.034	-0.098	-0.068	0.01	-1.453
7680 _D	0.010	0.028	-0.117	-0.095	0.02	-1.444
7680 _S	0.010	0.026	-0.120	-0.094	0.02	-1.443
7680 _D	0.010	0.019	-0.143	-0.128	0.03	-1.431
7680 _S	0.010	0.019	-0.143	-0.128	0.03	-1.432
7680 _S	0.025	0.037	-0.123	-0.082	0.01	-1.447
7680 _D	0.025	0.029	-0.141	-0.115	0.02	-1.437
7680 _S	0.025	0.029	-0.137	-0.115	0.02	-1.438
7680 _S	0.025	0.023	-0.160	-0.144	0.03	-1.425
7680 _S	0.050	0.041	-0.133	-0.097	0.01	-1.442
7680 _S	0.050	0.035	-0.143	-0.127	0.02	-1.432
7680 _S	0.050	0.032	-0.159	-0.152	0.03	-1.421
7680 _S	0.100	0.047	-0.119	-0.118	0.01	-1.437
7680 _S	0.100	0.051	-0.134	-0.132	0.02	-1.425
7680 _S	0.100	0.050	-0.150	-0.150	0.03	-1.415
7680 _S	0.250	0.021	-0.118	-0.108	0.01	-1.446
7680 _S	0.250	0.040	-0.123	-0.134	0.02	-1.428
7680 _S	0.250	0.069	-0.127	-0.145	0.03	-1.406
7680 _S	0.500	0.015	-0.140	-0.082	0.01	-1.440
7680 _S	0.500	0.027	-0.112	-0.151	0.02	-1.428
7680 _S	0.500	0.038	-0.147	-0.147	0.03	-1.416
7680 _D	1.000	0.018	-0.219	+0.031	0.01	-1.416
7680 _S	1.000	0.024	-0.336	+0.207	0.01	-1.390
7680 _D	1.000	0.029	-0.134	-0.141	0.02	-1.417
7680 _S	1.000	0.025	-0.200	-0.049	0.02	-1.413
7680 _D	1.000	0.042	-0.188	-0.135	0.03	-1.402
7680 _S	1.000	0.036	-0.184	-0.122	0.03	-1.407

of these results, with qualitative features sensitive to the form of the force law, suggests that simple analytical models, based on competing surface energy, strain energy, and kinetic energy, are too naïve to be useful in understanding constitutive data. Data for engineering materials are further complicated by the rôle played by impurities.

Such a model could be developed by imagining that shear causes grains to form, with a characteristic size L . The specific energy then deviates from the equilibrium value e_0 through (1) surface energy, (2) kinetic energy associated with the strain rate, and (3) stored elastic energy proportional to the square of the yield stress Y :

$$e = e_0 + (2\sigma/\rho L) + (L^2 \dot{\epsilon}^2)/12 + Y^2/2\rho G .$$

Table 3

Dependence of the stress tensor and energy on strain rate and temperature for simulations with 7763 particles ($\alpha = 1$ and density 1.213). K represents the kinetic temperature per particle. The subscripts D and S indicate the simulation type, Doll's or Silod. The individual run lengths are to a time of 240, with the first 40 time units discarded

N	$\dot{\epsilon}$	σ_{xy}	σ_{xx}	σ_{yy}	K	Φ
7763 _D	0.005	0.065	-0.063	-0.037	0.01	-1.488
7763 _D	0.005	0.049	-0.089	-0.065	0.02	-1.480
7763 _D	0.005	0.041	-0.117	-0.092	0.03	-1.470
7763 _D	0.010	0.070	-0.071	-0.045	0.01	-1.484
7763 _S	0.010	0.068	-0.067	-0.050	0.01	-1.484
7763 _S	0.010	0.054	-0.094	-0.075	0.02	-1.476
7763 _S	0.010	0.046	-0.127	-0.097	0.03	-1.465
7763 _S	0.025	0.076	-0.079	-0.065	0.01	-1.473
7763 _D	0.025	0.057	-0.108	-0.086	0.02	-1.466
7763 _S	0.025	0.061	-0.109	-0.085	0.02	-1.466
7763 _D	0.025	0.048	-0.137	-0.111	0.03	-1.456
7763 _D	0.050	0.073	-0.111	-0.056	0.01	-1.464
7763 _D	0.050	0.058	-0.126	-0.087	0.02	-1.457
7763 _D	0.050	0.046	-0.146	-0.118	0.03	-1.447
7763 _S	0.100	0.073	-0.122	-0.057	0.01	-1.454
7763 _D	0.100	0.062	-0.130	-0.091	0.02	-1.447
7763 _S	0.100	0.063	-0.130	-0.090	0.02	-1.446
7763 _S	0.100	0.056	-0.145	-0.120	0.03	-1.437
7763 _D	0.250	0.043	-0.119	-0.100	0.01	-1.468
7763 _D	0.250	0.056	-0.124	-0.116	0.02	-1.444
7763 _D	0.250	0.078	-0.125	-0.119	0.03	-1.423
7763 _S	0.500	0.032	-0.160	-0.041	0.01	-1.448
7763 _D	0.500	0.027	-0.144	-0.125	0.02	-1.453
7763 _D	0.500	0.047	-0.165	-0.127	0.03	-1.436
7763 _D	1.000	0.016	-0.13	-0.10	0.01	-1.455
7763 _D	1.000	0.029	-0.144	-0.129	0.02	-1.440

Minimization of the energy with respect to the grain size gives a relation between the strain rate and grain size of the same form as Rayleigh's relation for the vibrational frequency of an elliptical drop of radius R [15]:

$$\dot{\epsilon} = (24\sigma/\rho L^3)^{1/2}; \quad \omega = (6\omega/\rho R^3)^{1/2}.$$

For a fixed yield strength, these ideas suggest that the energy should increase as the $\frac{2}{3}$ power of the strain rate:

$$e = A + B\dot{\epsilon}^{2/3}.$$

In fact, the data for $T = 0.02$ indicate that the potential energy first rises, presumably with a decreasing grain size, and then undergoes a hysteretic decrease followed by an increase, as shear bands are formed.

5. Models for solid plasticity

Anisotropic plasticity can be described by models ranging from a simple equivalent yield criterion to those based on the motion of individual dislocations moving within developing anisotropic grains. Although these latter analyses are intrinsically most interesting, their complexity, even in two-dimensional situations, is already too elaborate for applications to macroscopic flows [14]. In the present case a detailed model of our results would separate the system into individual grains, each described by time-dependent basis vectors and an overall elastic stress tensor, with the grains exerting torques upon their neighbors through surface regions characterized by high-energy and large stress gradients.

A macroscopic approach is considerably simpler and should also be adequate for applications. We find a yield strength of order $C_{44}/20$, with a slight negative stress rotation and with an energy increase of at most a few percent over that of the perfect unstrained crystal. Evidently a useful description of the granular flow properties can be based on a correlation linking the two shear moduli to the observed yield strength. There is no obvious way to define direction-dependent single-crystal yield strengths except for perfect crystals, where such yield strengths are considerably higher.

Recent work has established that smooth-particle techniques can describe two-phase equilibria between fluids [18]. A similar approach could be applied to the present model, making more macroscopic simulations of temperature-sensitive flow phenomena possible.

6. Conclusions

Although the embedded-atom model provides a relatively simple means to stabilize elastically anisotropic solids, the constitutive behavior of these models is quite unlike that found earlier with simple pair potentials. The relatively easier slip, and lack of dependence of the stress on the strain rate are in accord with intuitive ideas of metallic flows. The relatively small energies associated with the grain boundaries and defects, as well as the absence of vacancies, except at very high strain rates, are likewise quite consistent with expectations for metals.

Stable grain morphologies are generated by either Dolls's or Sllod shear deformation, with an observed yield strength considerably lower than the lesser shear modulus C_{44} . Reliable stresses can be obtained with a few thousand particles, in two dimensions, corresponding to a few hundred thousand in three dimensions. There is no significant difference between the two algorithms. We believe that these results can be used with confidence and that corresponding three-dimensional simulations, with 100 000 particles, would lead to corresponding results. Additional two-dimensional simulations, in order to explore the sensitivity of the solid-phase flows to impurities and inhomogeneities inherent in the freezing process, would be welcome.

Acknowledgements

This work began at the Technical University of Berlin under a Materials Science Grant from Helmut Kohl via the Sonderforschungsbereich 335 "Anisotrope Fluide". Corresponding work in Livermore was performed under the auspices of the University of California, through Department of Energy contract W-7405-eng-48, under the Manufacturing Initiative for Advanced Scientific Computing, in the Department of Mechanical Engineering at the Livermore Laboratory. We specially thank our colleagues Carol Hoover, Roger Logan, Peter Raboin, and Dave Sam, for support, advice, and criticism. We specially thank our colleagues, Carol Hoover and Peter Raboin, for support, advice, and criticism.

References

- [1] B.L. Holian, in: K. Binder, G.P.F. Ciccotti (Eds.), *Monte Carlo and Molecular Dynamics of Condensed Matter Systems*, Editrice, Bologna, 1995, p. 881.
- [2] W.C. Sandberg, U. Obeysekare, C. Williams, A. Qasba, *Phys. Chem. Liquids* 35 (1997) 67.
- [3] B.L. Holian, P.S. Lomdahl, S.Y. Zhou, *Physica A* 240 (1997) 340.
- [4] M.S. Daw, M.I. Baskes, *Phys. Rev. B* 29 (1984) 6443.
- [5] B.L. Holian, A.F. Voter, N.J. Wagner, R.J. Ravelo, S.P. Chen, W.G. Hoover, C.G. Hoover, J.E. Hammerberg, T.D. Dontje, *Phys. Rev. A* 43 (1991) 2655.
- [6] W.G. Hoover, A.J. De Groot, C.G. Hoover, *Comput. Phys.* 6 (1992) 155.
- [7] J.J. Monaghan, *Ann. Rev. Astron. Astrophys.* 30 (1992) 543.
- [8] L. Lucy, *Astron. J.* 82 (1977) 1013.
- [9] Wm.G. Hoover, S. Hess, *Physica A* 231 (1996) 425.
- [10] W.G. Hoover, A.C. Holt, D.R. Squire, *Physica* 44 (1969) 437.
- [11] S. Hess, M. Kröger, W.G. Hoover, *Physica A* 239 (1997) 449.
- [12] W.G. Hoover, B. Moran, A.J.C. Ladd, *Phys. Rev. Lett.* 48 (1982) 1818.
- [13] B.L. Holian and P.S. Lomdahl, *Science* 280 (1998) 2085.
- [14] U.F. Kocks, C.N. Tomé, H.R. Wenk, *Texture and Anisotropy*, Cambridge University Press, Cambridge 1998 (Chapter 8).
- [15] W.G. Hoover, *Physica A* 260 (1998) 244.
- [16] W.G. Hoover, *Computational Statistical Mechanics*, Elsevier, Amsterdam, 1991.
- [17] D.J. Evans, G.P. Morriss, *Statistical Mechanics of Nonequilibrium Liquids*, Academic Press, New York, 1990.
- [18] T. Okuzono, *Phys. Rev. E* 56 (1997) 4416.